Protective Iron Carbonate Films—Part 3: Simultaneous Chemo-Mechanical Removal in Single-Phase Aqueous Flow

V. Ruzic,‡, M. Veidt,** and S. Nešić****

ABSTRACT

The service life of mild steel equipment found in the oil and gas production and transportation industry is often conditional on the viability of protective iron carbonate films. Once deposited on steel surfaces as by-products of the carbon dioxide corrosion process, their integrity may be severely affected by the influence of mechanical and/or chemical film removal. In this work, the investigation of simultaneous chemo-mechanical film removal has been undertaken to shed more light on the underlying conjoint mechanism. In addition, it provided the necessary information for the trilateral comparison with existing, available data on decoupled, single removal mechanisms. A rotating cylinder geometry has been utilized to create highly turbulent, undersaturated flow conditions at two Reynolds numbers (Re = 1.29 × 10^5 and 1.84 × 10^5) and pH 5.8. Film removal rates were followed by using the linear polarization resistance technique, while the film damage assessment was carried out by means of scanning electron microscopy. The findings clearly confirmed the correctness of the hypothesis on the synergism between the mechanical and chemical film removal mechanisms in single-phase flows. A likely mechanism was formulated for the simultaneous chemo-mechanical film removal process.

KEY WORDS: carbon dioxide corrosion, chemical film dissolution, mechanical film removal, protective iron carbonate film, rotating cylinder electrode, synergistic effect, turbulent single-phase flow

INTRODUCTION

Protective iron carbonate ($FeCO_3$) films are advantageous by-products of the carbon dioxide (CO_2) corrosion process that deposit on the parent metal and shield it from further damage. However, when the film is damaged, this may lead to costly failures of the mild steel equipment utilized in the oil and gas industry. The recent studies have indicated that two independent mechanisms can be responsible for $FeCO_3$ film disruption in an undisturbed single-phase flow: mechanical removal by hydrodynamic forces[1] and chemical removal by dissolution.[2]

It is well known that in multiphase flow (e.g., liquid droplet impingement, bubble cavitation, solid particle erosion, etc.) films are removed primarily by mechanical "impact" forces.[3] The same appears to be true for submerged impinging jets where the liquid flow impinges perpendicularly on the metal surface.[4-6] It seems that, in all of these cases, the hydrodynamic forces are generally capable of overcoming the mechanical resistance of the protective film. However, in single-phase flow through pipes and fittings, the film removal process frequently has been associated exclusively with chemical dissolution.[3,7] Indeed, it was considered that in single-phase aqueous flow, for typical velocities seen in practice (<10 m/s), the removal of protective films could not be induced mechanically by hydrodynamic forces alone because they were consid-

Submitted for publication August 2005; in revised form, April 2007. Part 1 of this manuscript appears in *Corrosion* 62, 5 (2006), p. 419-432. Part 2 appears in *Corrosion* 62, 7 (2006), p. 598-611.

‡ Corresponding author. E-mail: v.ruzic@mptsolutions.com.

* Department of Mechanical Engineering, The University of Queensland, Brisbane Queensland 4072, Australia. Present address: MPT Solutions Pty Ltd, Brisbane Technology Park, 2/53 Brandl St., PO Box 4551, Eight Mile Plains Queensland 4113, Australia.

** Department of Mechanical Engineering, The University of Queensland, Brisbane Queensland 4072, Australia.

*** Institute for Corrosion and Multiphase Flow Technology, Chemical Engineering Department, Ohio University, 340½ W. State St., Stocker Center, Athens, OH 45701.

0010-9312/07/000133/$5.00+$0.50/0

ered to be too small. However, Ruzic, et al., have recently documented that pure mechanical film removal in undisturbed, single-phase aqueous flow is possible.[1] Pure mechanical breakdown of $FeCO_3$ films in aqueous solutions was reported earlier by Schmitt, et al.,[8] who used a "rotating cage" flow geometry, which creates very violent flow conditions and certainly does not qualify as undisturbed flow. The critical mean wall shear stress (τ_w) was often stated traditionally as an important factor responsible for mechanical material loss.[4,9-10] However, the current findings recognize that the mean wall shear stress is too small to be the dominant contributor.[1,8] Instead, local turbulence/microturbulence levels accompanied by significant fluctuation quantities,[1,5-6] as well as the internal intrinsic stresses[8] in some instances, have been proposed to play major roles in mechanical film destruction.

On the other hand, there seems to be a consensus that chemical dissolution mechanism is mass-transfer-controlled.[2,11-14] The $FeCO_3$ dissolution reaction is defined as:

$$FeCO_3(s) \Rightarrow Fe^{2+} + CO_3^{2-} \quad (1)$$

It is well known that the protective film readily dissolves when subjected to unsaturated solutions (S < 1). The saturation (S) may be expressed as:

$$S = \frac{[Fe^{2+}][CO_3^{2-}]}{K_{sp}} \quad (2)$$

where [ ] denotes equilibrium concentration of the species, and K_{sp} is the solubility product dependent on temperature and electrolyte ionic strength. It has been suggested that film dissolution does not proceed uniformly; rather, it occurs through selective dissolution and via pore creation by dissolution of crystalline surface asperities, which enables direct dissolution of the amorphous inner film layers.[2]

In practical applications, such as, for example, pipeline transportation of crude oil and gas, where pH typically varies between 4 and 6,[15] it is thought that the parallel action of both removal mechanisms could be at play. Vyas has hypothesized that mechanical and chemical processes acting together may be more damaging than if they act separately, suggesting the synergistic effect between the two.[16] Some evidence for this can be found in the work of Giralt and Trass, who pointed out that the dissolution led to the loosening of film crystal grains, rendering them more prone to mechanical erosion.[4,11] However, many investigations that dealt with synergistic phenomena often lacked properly defined and strictly controlled experimental conditions for both mechanisms, which may have led to a misleading interpretation of results. For example, in the case of the otherwise excellent study of Giralt and Trass,[4,11] the pure dissolution in the absence of erosion was not measured, probably due to the fact that impact forces could not have been eliminated in a jet impingement testing environment. As a consequence, the relative contributions of mechanical film erosion and dissolution could not be separated. Yet, their work, which was done by using a model coating material (trans-cinnamic acid [$C_9H_8O_2$]), is still significant and unique in the sense that it took into consideration simultaneous mechanical removal and chemical dissolution—the two pertinent film removal mechanisms. No other similar studies are available to date that are done with more realistic corrosion films or scales. On the other hand, there are numerous examples in the open literature where the combined effect of corrosion and mechanical erosion by solid particles in two-phase flows was studied.[17-20] In most of these so-called slurry erosion-corrosion or abrasion-corrosion studies, an agreement has been reached that metal loss regime is erosion-dominated. However, the contradictory results have been reported with respect to the governing synergistic mechanism: erosion-assisted corrosion[18] vs. corrosion-assisted erosion.[20]

The present work is the last in the trilogy including the two preceding papers that dealt with individual decoupled $FeCO_3$ removal mechanisms, i.e., mechanical film removal[1] (M) and chemical film dissolution[2] (D). Therefore, a series of experiments with combined mechanical film removal and chemical film dissolution (CMD) in undisturbed single-phase flow, i.e., simultaneous chemo-mechanical attack as it will be also referred to in this text, was carried out with a goal to verify if there is any synergism involved.

EXPERIMENTAL PROCEDURES

A classical three-electrode glass cell arrangement was utilized for the CMD experimental series. Tubular specimens, outer diameter (OD) by height (H) (12 mm by 10 mm), produced from 1020 mild steel (UNS G10200)[(1)] and mounted onto the rotating cylinder (RC) acted as a working electrode (WE). The electrochemical configuration was complemented by a 0.7-mm annular platinum wire, which served as a counter electrode (CE), while a saturated silver/silver chloride (Ag/AgCl) electrode was used as a reference electrode (RE). The operating conditions were 80°C and atmospheric pressure (101 kPa), at which the partial pressure of CO_2 gaseous phase was p_{CO_2} = 0.54 bar. Because film removal rates are difficult to measure directly in mol/m^{2}s, they were followed implicitly via measuring the corrosion rates (CR) by using the linear polarization resistance (LPR) method. After the experiments, the damage characterization, i.e., the assessment of film morphology, thickness,

[(1)] UNS numbers are listed in *Metals and Alloys in the Unified Numbering System*, published by the Society of Automotive Engineers (SAE International) and cosponsored by ASTM International.

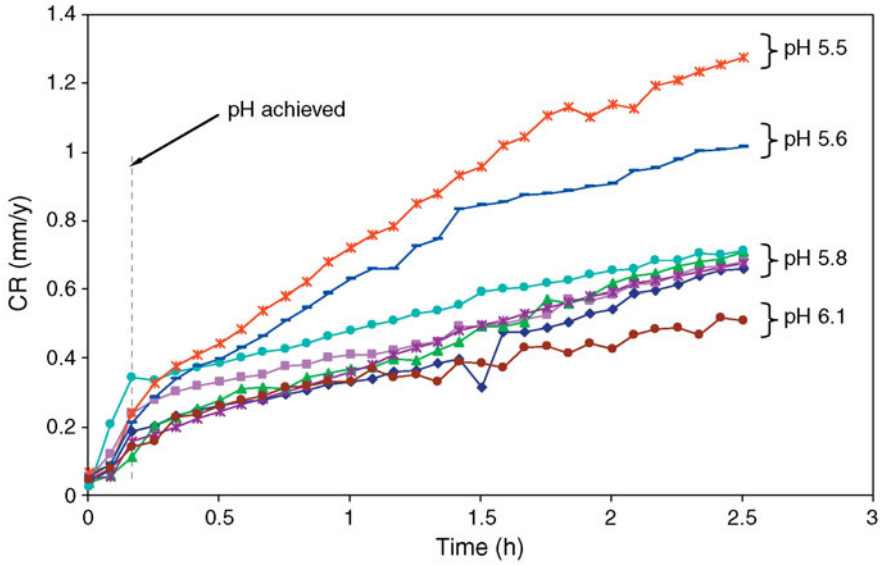

FIGURE 1. *CR increase during CMD film removal at 10,000 rpm for pH 5.5 to 6.1, T = 80°C, p_{CO_2} = 0.54 bar, and 1 wt% sodium chloride (NaCl), where t = 0 h corresponds to the onset of CMD removal following the mechanical initiation period.*

damage type, etc., was carried out by means of scanning electron microscopy (SEM).

Film Formation

The film was formed in less than 2 days by precipitation at 200 rpm rotational speed (v = 0.13 m/s specimen peripheral velocity; Re = 3.68 × 10^3). The film was typically very protective (CR < 0.05 mm/y) as well as smooth and uniformly thick (≈50 μm). The preferred film formation procedure was "type B" as described in detail previously.[1-2] More on the equipment, solution, and specimen preparation procedures, as well as the film growth methodology, can be found in Ruzic, et al.[1]

Chemo-Mechanical Film Removal

Since the in-depth explanation of pure mechanical[1] and chemical[2] film removal procedures are given elsewhere, this section only describes procedural amendments that were necessary to make in order to obtain simultaneous chemo-mechanical attack.

Once a very protective film had formed, the rotational speed was increased to match the same turbulent conditions as used in the studies of the decoupled film removal mechanisms, i.e., 7,000 rpm (v = 4.40 m/s; Re = 1.29 × 10^5) and 10,000 rpm (v = 6.28 m/s; Re = 1.84 × 10^5), and induce mechanical stress on the film. Shortly after, film dissolution was initiated by changing the water chemistry from a supersaturated to an unsaturated solution by adding hydrochloric acid (HCl). To match the short exposure times used in the pure dissolution experimental series, experiments were stopped after 2.5 h.

The LPR potential sweeps were performed by polarizing the WE ±20 mV relative to the open-circuit potential (E_{oc}) with a fast scan rate (0.5 mV/s) every 10 min during the mechanical damage initiation period and then every 5 min upon the introduction of dissolution.

The bulk solution Fe^{2+} concentration $[Fe^{2+}]_b$ samples were taken at various times: 0 h (at the onset of mechanical film removal), 0.17 h (after pH adjustment), 1.33 h (midway through the experiment), and at 2.5 h (end of experiment). Fe^{2+} concentration was analyzed by using the phenanthroline calorimetric method. The corresponding pH value in the solution was measured for each acquired $[Fe^{2+}]_b$ sample. Finally, after the experiment had been conducted, the specimens were dried and prepared for cross-sectional and topographic SEM examination.

RESULTS

Effect of pH

The effect of simultaneous mechanical film removal and dissolution for a range of pH values is illustrated in Figure 1. It should be noted that for the sake of easier comparison the time has been normalized with respect to the introduction of dissolution, i.e., time t = 0 h corresponds to the onset of chemo-mechanical film removal following the mechanical initiation period. A faster CR increase was observed for the higher acid concentrations, as expected. The pH adopted for all subsequent experiments was pH 5.8, because of good reproducibility and a linear increase in the corrosion rate, suggesting a steady removal of the protective film. In addition, this pH was suitable for comparisons with previously obtained data for decoupled mechanical film removal[1] and dissolution.[2]

TABLE 1
Summary of Main Chemo-Mechanical Film Removal Results at pH 5.8[A]

Rotational Speed (rpm)	Mean Final CR (mm/y)	Mean CR_{grad} (mm/y/h)	Mean Initiation Time (CMD) (h)	Corrected Mean Initiation Time (CMD and M) (h)	Mean Final Steady-State E_{corr} (V)
7,000	0.29 ± 0.01	0.0630 ± 0.0031	8.3 ± 1.6	7.6 ± 1.1	–0.685 ± 0.007
10,000	0.69 ± 0.01	0.2022 ± 0.0117	4.6 ± 0.7	4.5 ± 0.5	–0.706 ± 0.002

[A] Experimental uncertainties represent standard deviation of the mean, i.e., standard error.

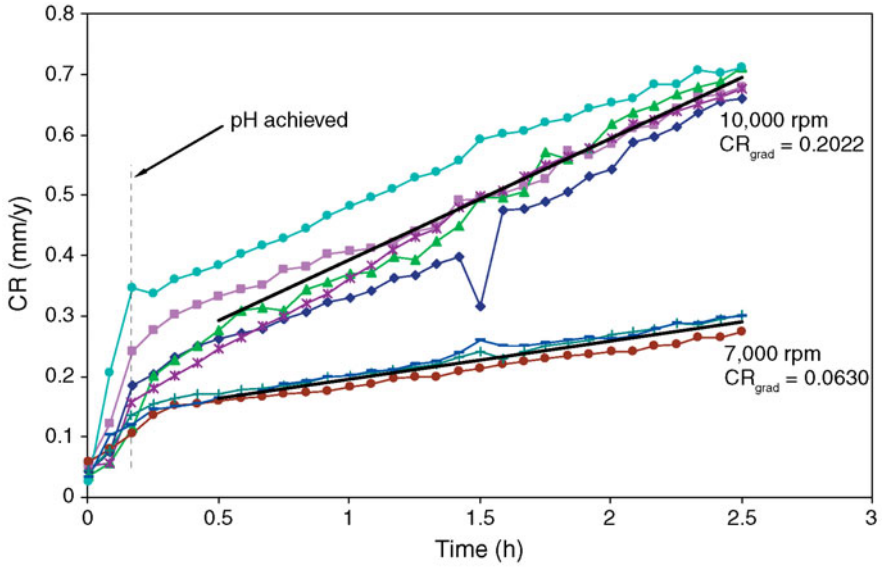

FIGURE 2. *CR increase during CMD film removal at pH 5.8 for 10,000 rpm and 7,000 rpm, T = 80°C, p_{CO_2} = 0.54 bar, and 1 wt% NaCl, where t = 0 h corresponds to the onset of CMD removal following the mechanical initiation period.*

Effect of Velocity

The effect of velocity was studied at two rotational speeds: 7,000 rpm and 10,000 rpm. These matched the conditions used in experiments where decoupled mechanical film removal[1] and dissolution[2] were measured. The summary of the results discussed in this section is tabulated in Table 1.

In Figure 2, one can observe that the film removal kinetics (as indicated by the slope of the CR increase curve) and the final CRs were reproducible. A steady-state linear CR increase established by the 0.5-h mark remained preserved until the end of experiment for both velocities. Furthermore, at higher velocity the rate of film removal was higher, as one would expect. The corresponding corrosion potential (E_{corr}) plots are presented in Figure 3. Interestingly, the E_{corr} experienced a rapid decrease during the acid concentration increase period (0 to 0.17 h) before any significant damage to the film could be identified from the CR measurements. The transient disturbances ("kinks" in the CR and E_{corr} curves) midway through the experiments (1.33 h) seen in Figures 1 through 3 were due to the flow perturbations caused by the immersion of various process-control and monitoring equipment. Figure 4 shows the corresponding measurements of ferrous ion concentration $[Fe^{2+}]_b$ in bulk solution.

The linear regression analysis using the least-squares method was carried out to fit the appropriate CR trend lines. The mean CR gradients (CR_{grad}), subsequently determined from the straight regression lines of best fit, are presented in Figure 2 and Table 1. The ratio of the mean CR gradients for the higher and lower velocities, called the CMD velocity "enhancement factor" here, was EF_{CMD} = 3.20, i.e., effectively, the film was removed more than three times faster at the higher velocity. When compared with the corresponding flow enhancement factors in decoupled mechanical film removal (EF_M = 2.08)[1] and film dissolution experiments (EF_D = 2.93),[2] the present number seems plausible.

Film Damage Characterization — As anticipated, SEM inspection confirmed the presence of the damage. Both types of damage were observed: film cracking in the vertical direction and spalling due to mechanical forces (M),[1] as well as formation of microscopic superficial pores on the top film layer and thinning of the inner film layer in the top-to-bottom direction due to

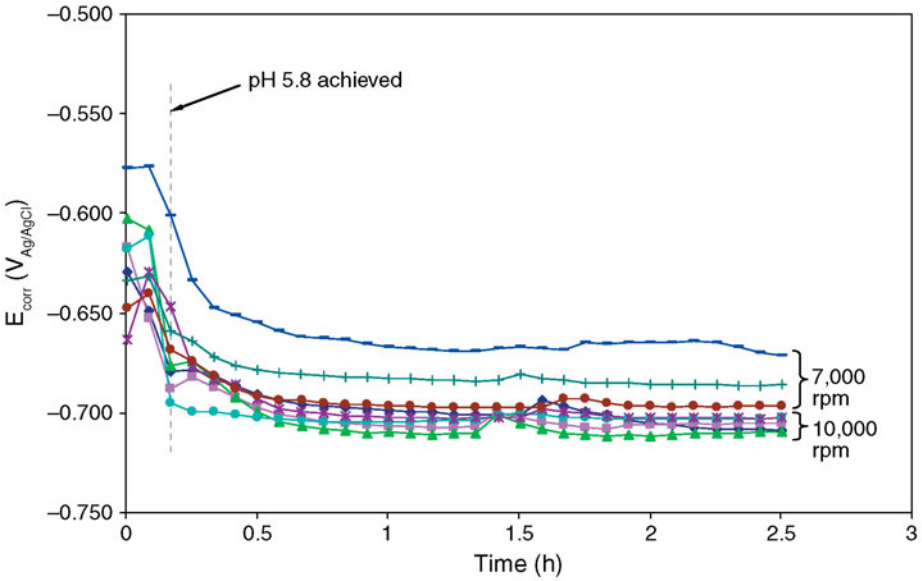

FIGURE 3. *Variation of E_{corr} with exposure time during CMD film removal at pH 5.8 for 10,000 rpm and 7,000 rpm, T = 80°C, p_{CO_2} = 0.54 bar, and 1 wt% NaCl, where t = 0 h corresponds to the onset of CMD removal following the mechanical initiation period.*

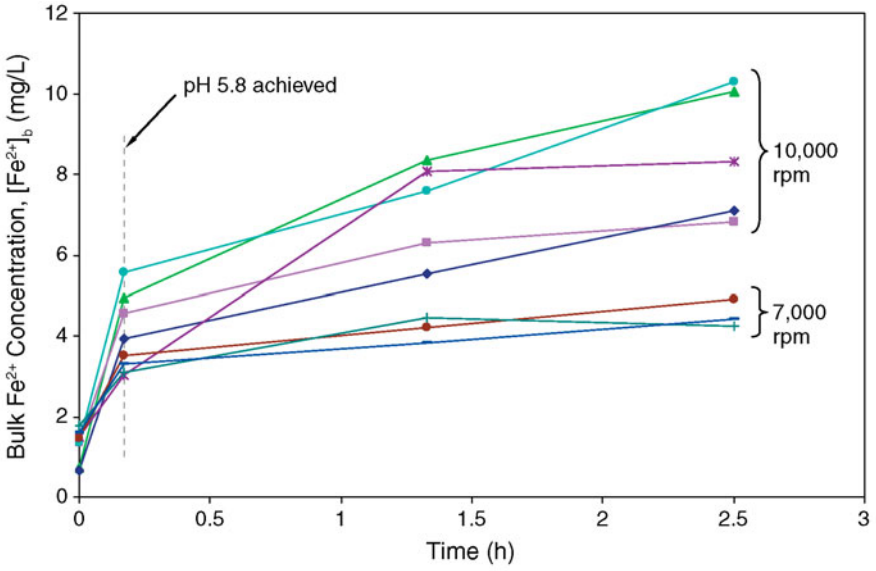

FIGURE 4. *Measured $[Fe^{2+}]_b$ rise in bulk solution during CMD film removal at pH 5.8 for: 10,000 rpm and 7,000 rpm.*

dissolution (D).[2] In addition, two modes of mutual interaction between the two base mechanisms were observed: dissolution-assisted mechanical removal (M/D) and mechanically assisted dissolution (D/M).

The cross-sectional areas of film residuals are shown in Figures 5 and 6 for 10,000-rpm and 7,000-rpm rotational speeds, respectively. As can be seen from Figure 5(a), there were areas where the film was removed entirely and other areas still covered by the film, similar to that observed in pure mechanical film removal.[1] However, in many places the surviving film was severely damaged, and often the top layers of the film were missing completely, exposing the inner film structure. These characteristics of the film are unique for CMD attack. Such "delamination" of the film layers was not seen in pure mechanical removal where patches of the film were removed entirely exposing the metal surface,[1] nor was it seen in pure dissolution at this pH.[2] Clearly, this M/D mode of CMD damage was due to the interaction of the two individual film removal mechanisms. The partial dissolution of the inner portions of the film weakened the "foundations" of the outer film, which then was removed by mechanical forces. This resulted in increased surface

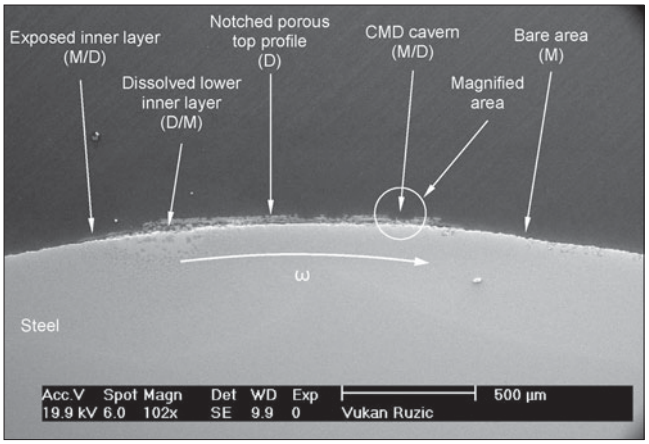

(a)

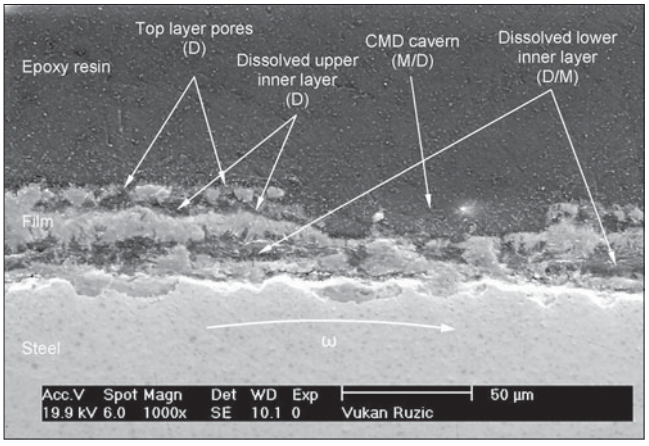

(b)

FIGURE 5. *Cross section of $FeCO_3$ film at the end of CMD film removal process at pH 5.8 and 10,000 rpm showing: (a) typical cross-sectional appearance (SE, magnification: 100X) and (b) magnified cavern site—area encircled in Figure 5(a) (SE, magnification: 1,000X).*

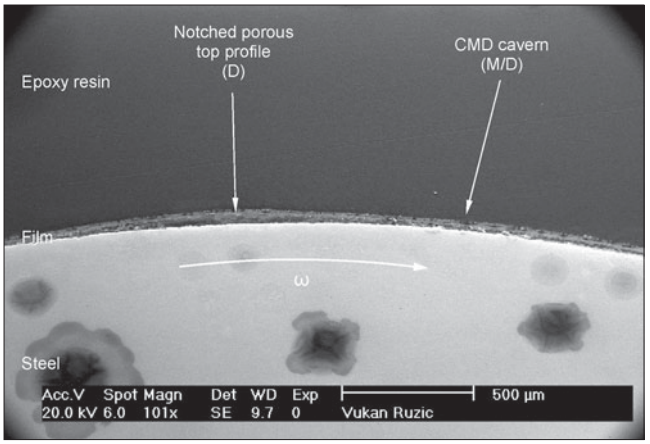

(a)

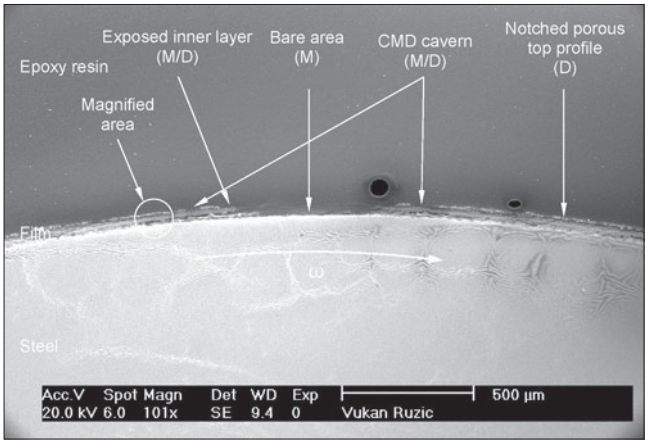

(b)

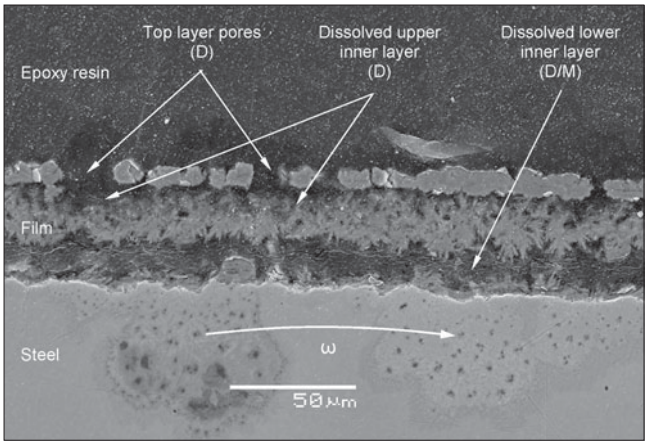

(c)

FIGURE 6. *Cross section of $FeCO_3$ film at the end of CMD film removal process at pH 5.8 and 7,000 rpm showing: (a) typical, film-covered appearance (SE, 100X), (b) atypical, film-free area (SE, 100X), and (c) typical appearance of the remaining film in the vicinity of a film-free area—area encircled in Figure 6(b) (SE, 1,000X).*

roughness at such sites and even more turbulence, leading to more damage in an "autocatalytic" fashion. On the other hand, in some instances, the dissolution damage to the inner film proceeded laterally from the bare areas previously created by mechanical attack, which led to further undermining of the remaining film, i.e., D/M damage mode (Figures 5 and 6[c]). Likewise, this feature was not observed in pure chemical removal at the same pH, where dissolution of the more dissolution-susceptible inner film layer occurred below the superficial pores on the top film layer in the top-to-bottom direction only.[2]

The topographic SEM micrographs for high (Figure 7) and low velocities (Figures 8 and 9) confirmed the characterization based on the cross-sectional images. All the qualitative findings are labeled in the figures for easy reference.

The features of pure dissolution component (superficial pores), which are similar in nature to what was reported previously by Ruzic, et al.,[2] could be observed clearly in secondary electron (SE) (Figure 7[b]) and back-scattered electron (BSE) (Figure 7[c]) images. The typical surface micrograph of the low-

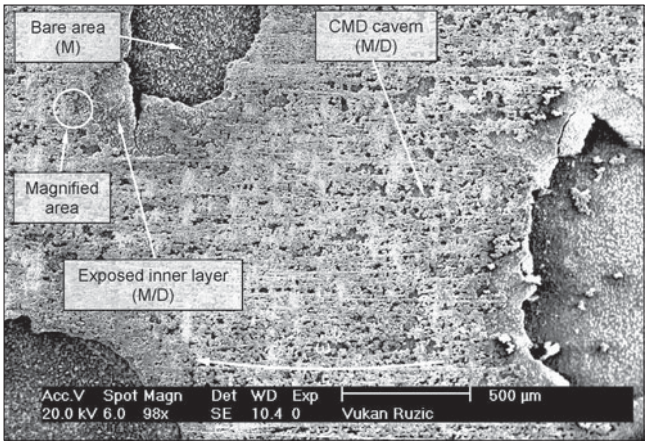

(a)

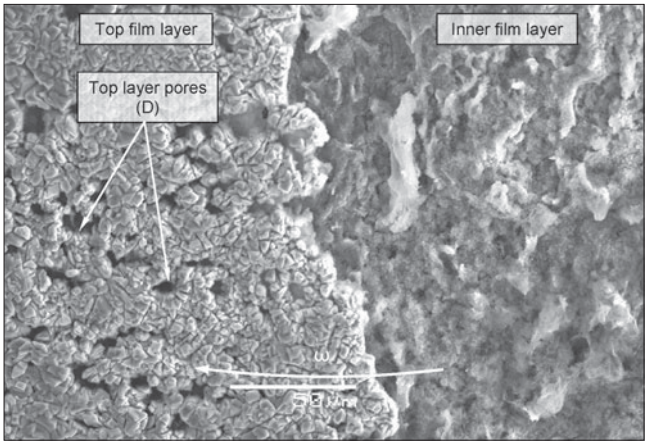

(b)

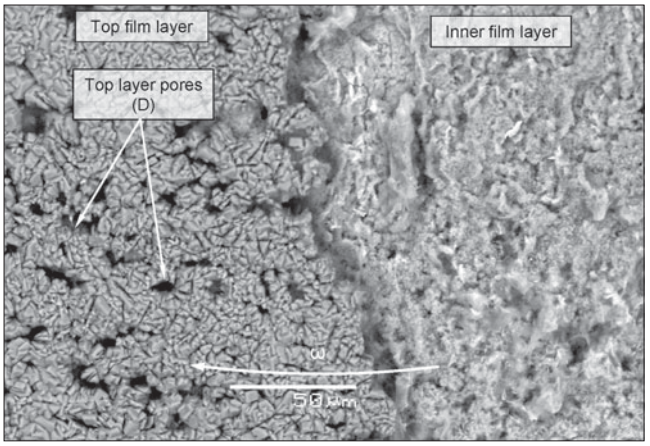

(c)

FIGURE 7. *Surface topography of $FeCO_3$ film at the end of CMD film removal process at pH 5.8 and 10,000 rpm showing: (a) typical surface appearance (SE, 100X) as well as magnified (b) (SE, 1,000X) and (c) (BSE, 1,000X) image of area encircled in Figure 7(a).*

velocity specimen (Figure 8[a]) revealed the presence of vertically oriented cracks along with clusters of pores. Figure 8(b) shows a magnified vertical crack surrounded by pores. A somewhat less typical low-velocity damage case features bare metal patches and other unique CMD removal characteristics (Figure 9[a]). The encircled area from Figure 9(a) is shown as SE and BSE images in Figures 9(b) and (c), respectively. Apart from the dissolution pores, the development of microcracking (M/D mode) as a result of CMD attack is clearly visible.

In summary, the appearance of the mechanical component in CMD film removal had some unique M/D features but was for the most part similar to what was observed in pure mechanical removal situations.[1] Yet, the main difference was in the kinetics—it took up to ten times longer to achieve the same degree of damage in the pure mechanical film removal experiments. Clearly, the film dissolution drastically accelerates and facilitates the mechanical film removal by undermining the adherent inner layer and by loosening the whole film chunks. In contrast, unhindered physical access and significantly larger film area exposed to the solution, both of which were the result of prior mechanical damage to the film, were responsible for the enhanced multidirectional dissolution of the inner film layer, i.e., D/M mode.

Effect of Exposure Time

A single, low-velocity experiment was prolonged until the stabilization of CR was achieved. As it was hoped that the mechanical removal initiation time would substantially reduce in the presence of dissolution due to the expected M/D effect, the experiment had been designed as an ordinary pure film dissolution test (i.e., the initiation period under the pure mechanical conditions was omitted), which was subsequently allowed to spontaneously progress until the CR showed a tendency to slow down. The acquired CR increase curve is given in Figure 10. The pure dissolution process dominated around the 2.5-h mark until the departure from linearity indicated that the onset of mechanical film removal had initiated at 3 h. The transition took 1 h before the steady, linear CMD film removal was fully established at 4 h. The linear trend was observed for the next 6 h followed by a slowdown in CR rise. Although the corrosion rate (CR = 1.21 mm/y) did not achieve a steady-state value by the termination point at 23.7 h, it definitely showed a pronounced decelerating trend toward CR leveling. The long-term CMD removal slope was 15% higher than the mean slope in the short-term experiments.

Film Damage Characterization — Typical surface damage pattern in the long-term experiment exhibited features of pure mechanical removal (M) as well as the M/D mode, as shown in the SE micrograph in Figure 11(a). The pores, which are characteristic of pure dissolution (D), are only noticeable from the BSE image in Figure 11(b) due to the small magnification used. Figure 12 (encircled region in Figure 11) testifies to the severity of M/D damage, showing three wide caverns. Further magnification of one of the caverns

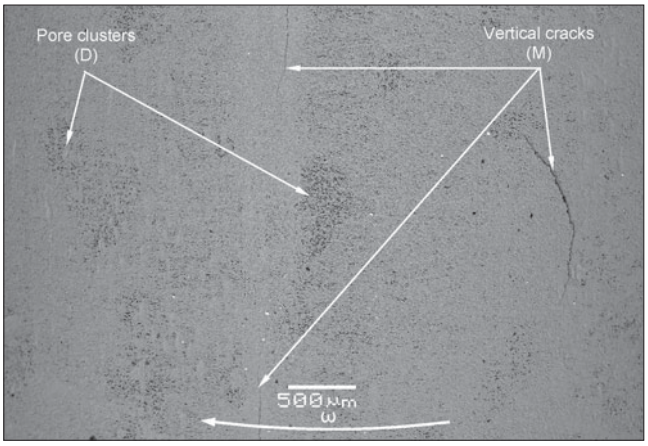

(a)

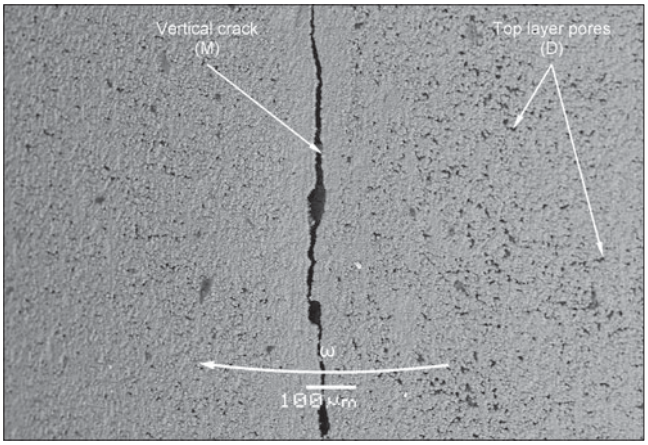

(b)

FIGURE 8. *Surface topography of $FeCO_3$ film at the end of CMD film removal process at pH 5.8 and 7,000 rpm showing: (a) typical surface appearance (BSE, 50X) and (b) magnified superficial, vertically oriented crack (BSE, 200X).*

(encircled region in Figure 12) is given in Figure 13. It shows many crystal grains with reduced size due to dissolution. Many of them have clearly lost their cubic shape and sharp edges and have become more rounded. Finally, the cross-sectional SEM micrograph of the least-affected film section is shown in Figure 14. The thinned and porous inner layer does not show good attachment to the top film layer nor the metal substrate, providing good evidence of the bidirectional thinning action, owing to the D/M mode. Such a vastly disintegrated film structure obviously could not provide any adequate protection to the underlying steel (final CR = 1.21 mm/y).

DISCUSSION

The mean CR increase (which indicates the film damage rate) for the combined chemo-mechanical mechanism was plotted along with the mean corresponding values at pure mechanical[1] and chemical[2]

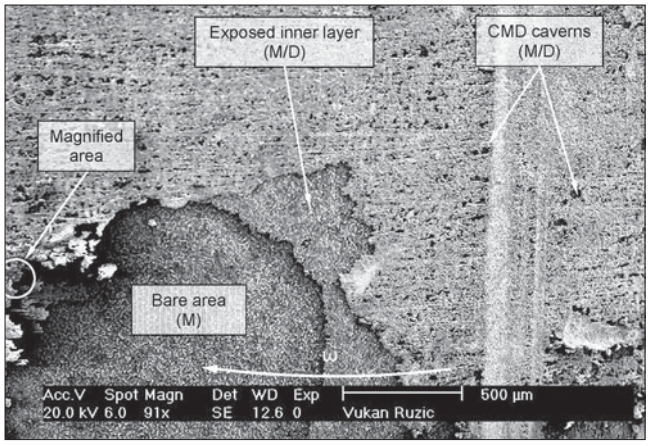

(a)

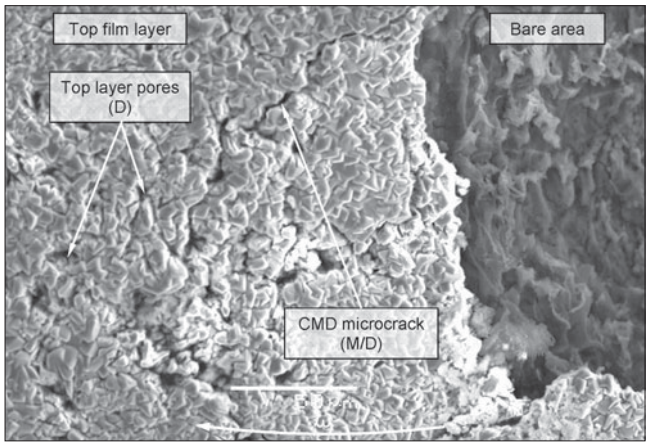

(b)

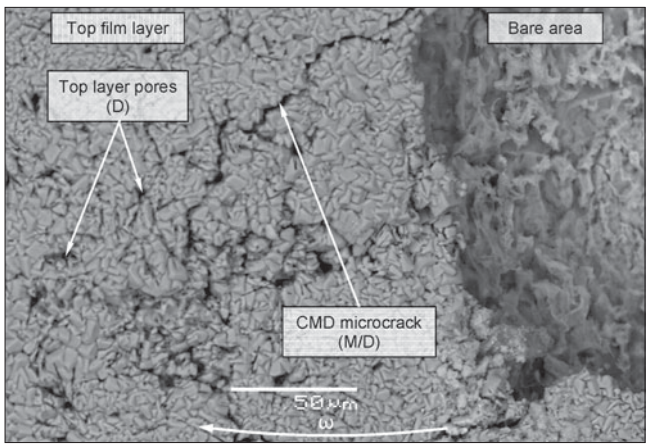

(c)

FIGURE 9. *Surface topography of $FeCO_3$ film at the end of CMD film removal process at pH 5.8 and 7,000 rpm showing: (a) atypical surface appearance (SE, 100X) as well as magnified (b) (SE, 1,000X) and (c) (BSE, 1,000X) image of area encircled in Figure 9(a).*

film removal for both velocities in Figure 15. It is clear from inspecting Figure 15 that when acting independently, film dissolution was more important than mechanical film removal under these conditions.

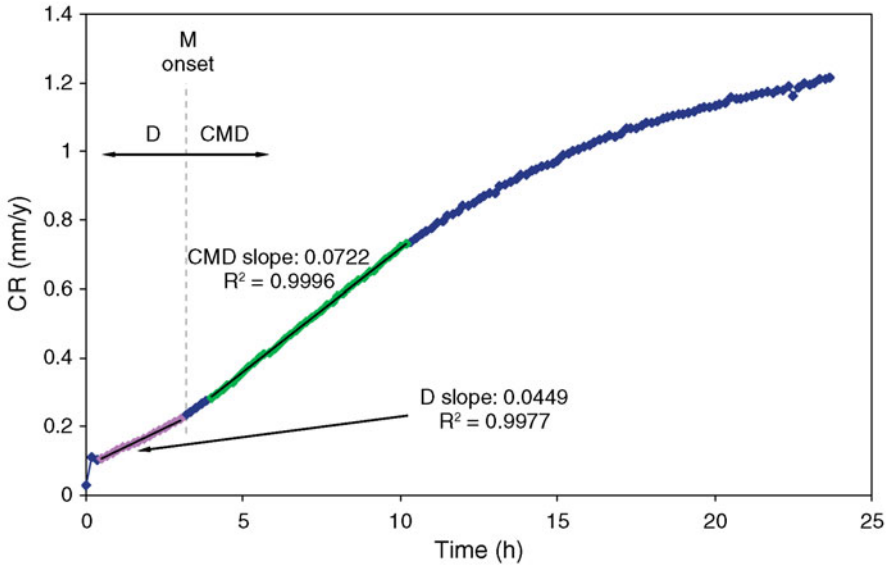

FIGURE 10. *CR increase during long-term CMD film removal following pure film dissolution process at pH 5.8, 7,000 rpm, T = 80°C, p_{CO_2} = 0.54 bar, and 1 wt% NaCl.*

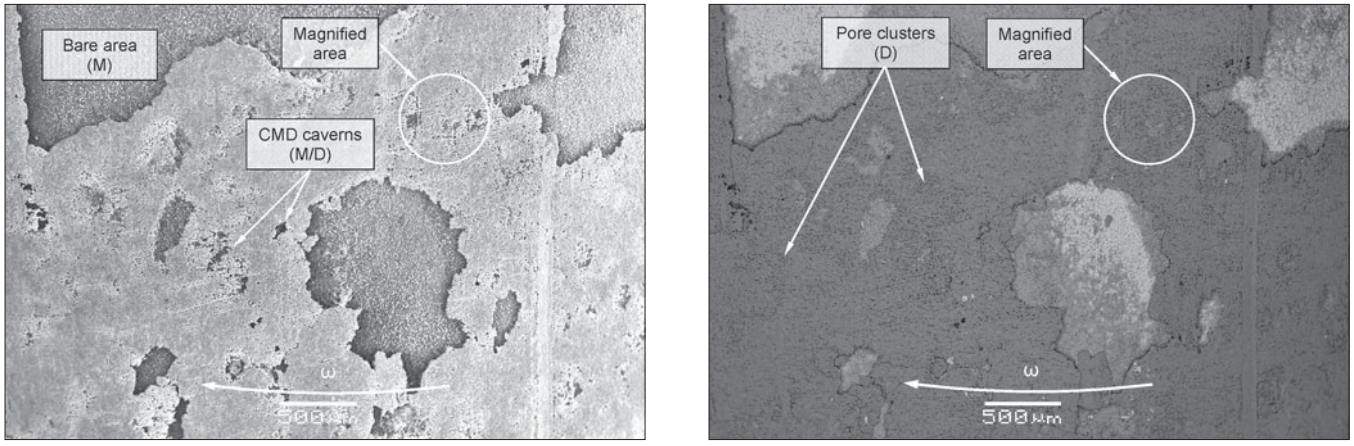

(a) (b)

FIGURE 11. *Typical surface topography of $FeCO_3$ film at the end of long-term CMD removal process at pH 5.8 and 7,000 rpm in: (a) SE and (b) BSE modes (magnification: 50X).*

Figure 16 shows the synergy between mechanical (M) and chemical dissolution (D) film removal mechanisms, i.e., that the combined chemo-mechanical removal action (CMD) yielded damage to the $FeCO_3$ film that was greater than the simple sum of its decoupled components:

$$CMD > M + D \Rightarrow CMD = (M + D) + \Sigma \quad (3)$$

where Σ represents the total synergistic effect. This synergistic effect was significant.

The total synergistic effect may be broken down further:

$$\Sigma = M/D + D/M \quad (4)$$

in which M/D is the effect of enhanced mechanical film removal due to dissolution, primarily reflected through accelerated mechanical removal kinetics, but also through unique M/D damage forms (top film layer stripping and wide caverns), and D/M is the effect of enhanced dissolution due to mechanical removal, mainly manifested through the enhanced multidirectional dissolution of the inner film layer.

The contribution of the synergism to the chemo-mechanical film removal process can be expressed by introducing the relative synergistic ratio (R):

$$R = \frac{\Sigma}{(M + D) + \Sigma} \quad (5)$$

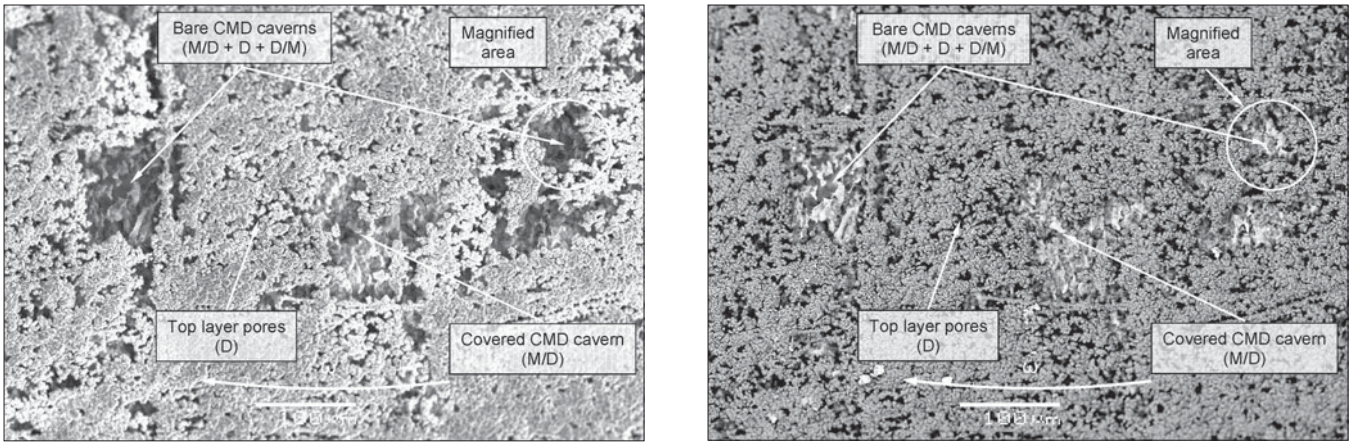

(a) (b)

FIGURE 12. *Surface topography of $FeCO_3$ film at the end of long-term CMD removal process at pH 5.8 and 7,000 rpm showing wide CMD caverns (magnified image of area encircled in Figure 11) in: (a) SE and (b) BSE modes (magnification: 400X).*

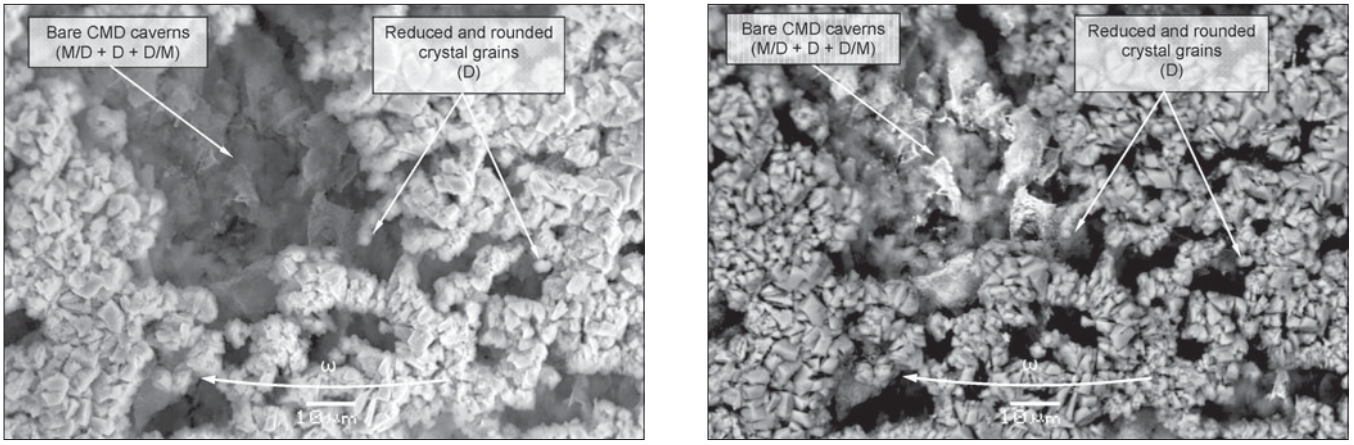

(a) (b)

FIGURE 13. *Surface topography of $FeCO_3$ film at the end of long-term CMD removal process at pH 5.8 and 7,000 rpm showing a wide CMD cavern (magnified image of area encircled in Figure 12) in: (a) SE and (b) BSE modes (magnification: 2,000X).*

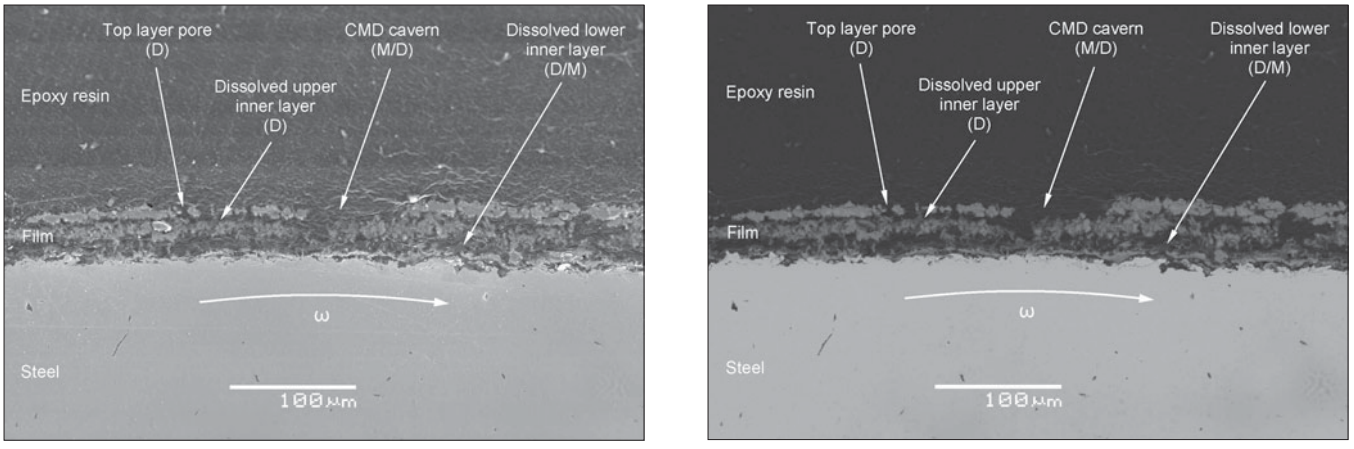

(a) (b)

FIGURE 14. *Cross section of $FeCO_3$ film at the end of long-term CMD removal process at pH 5.8 and 7,000 rpm showing typical film residual and wide CMD cavern in: (a) SE and (b) BSE modes (magnification: 500X).*

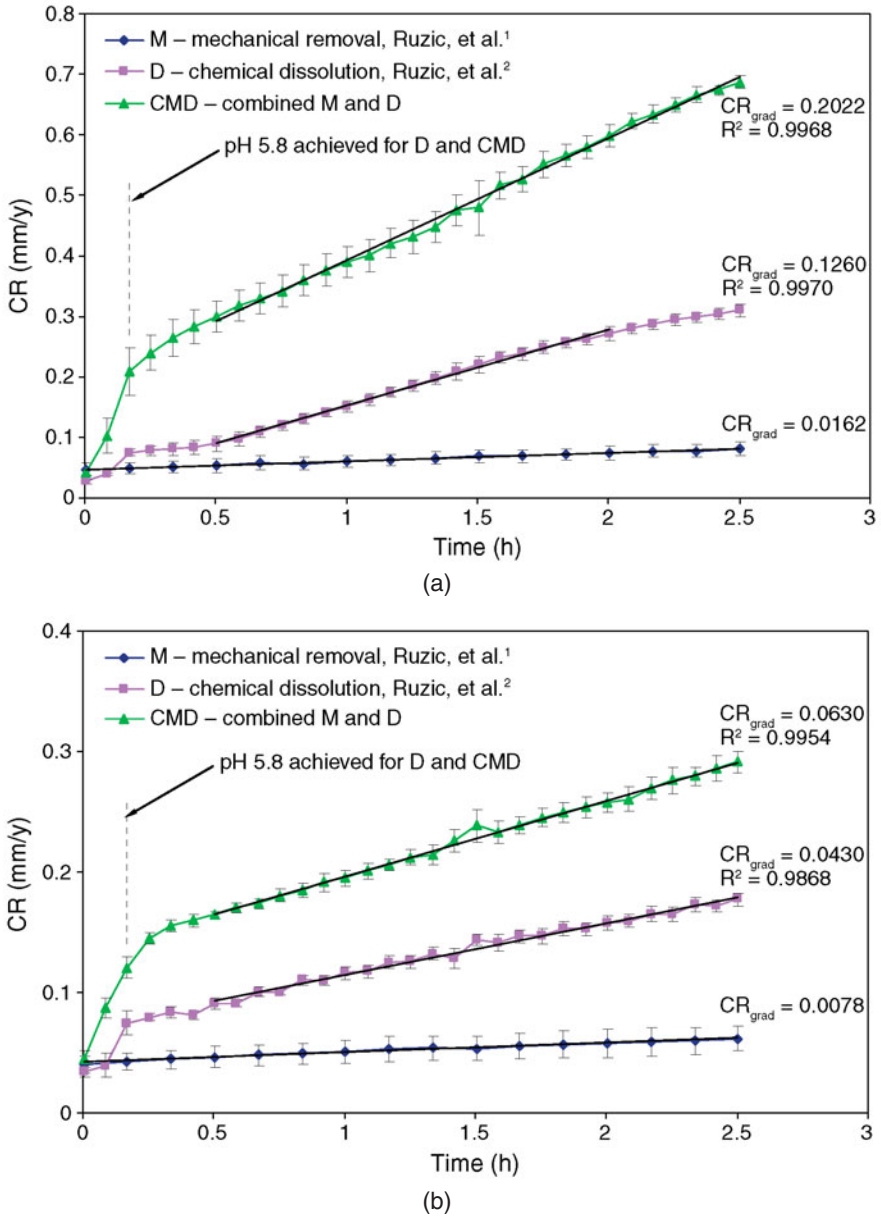

FIGURE 15. *Comparison of CMD attack and pure dissolution at pH 5.8 as well as pure mechanical film removal at pH 6.9 for: (a) 10,000 rpm and (b) 7,000 rpm (bars represent standard deviation of the mean, i.e., standard error).*

Figure 17 shows the evolution of the synergistic share in the chemo-mechanical removal with velocity. It is not only that the absolute intensity of the synergy showed very strong dependence on velocity (Figure 16), but its relative contribution in the CMD film removal mechanism also increased with flow rate (Figure 17).

CONCLUSIONS

The combined chemo-mechanical $FeCO_3$ film removal mechanism has been studied in undisturbed, highly turbulent rotating cylinder flow (Re = 1.29×10^5 to 1.84×10^5) at pH 5.8 and 80°C. The comparison of results with available data for decoupled pure mechanical removal[1] and dissolution[2] at the same conditions has shown the following:

❖ The synergistic effect has been identified between mechanical and chemical film removal mechanisms when the two acted simultaneously. The chemo-mechanical attack was found to be velocity-dependent. The same was true for the synergistic contribution, which increased with flow intensity, both in magnitude and in the relative contribution to the chemo-mechanical removal mechanism.

❖ The total synergistic effect is primarily manifested through significantly accelerated mechanical removal kinetics, enabled by enhanced multidirectional dis-

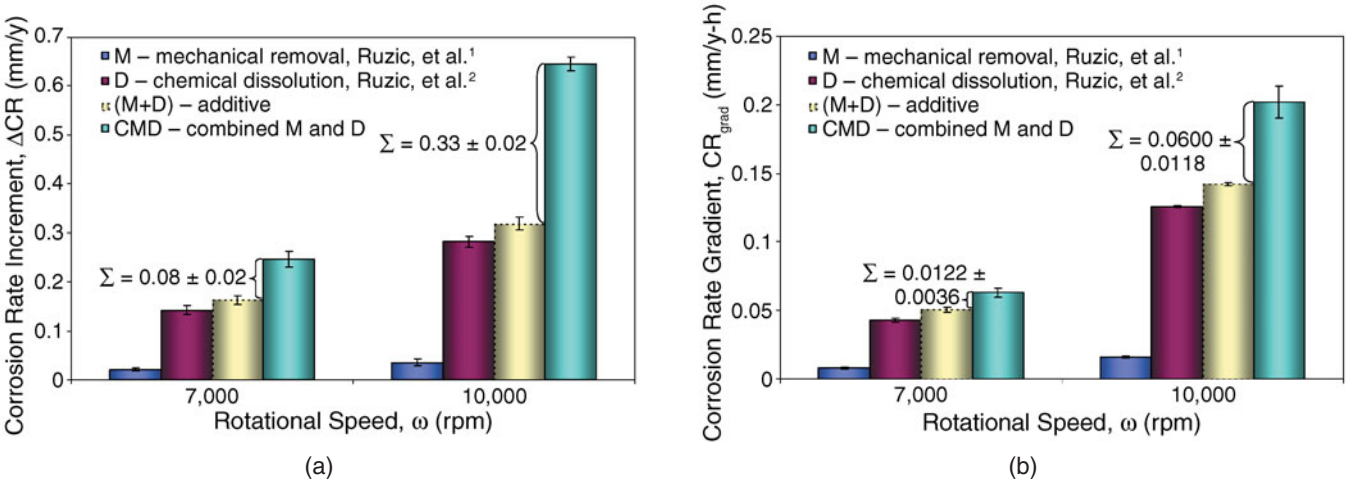

FIGURE 16. *Synergistic effect during the CMD attack at pH 5.8 expressed via: (a) CR increments (ΔCR) for the 2.5-h cut-off period and (b) steady, linear film removal rates implicitly followed by CR gradients (CR_{grad}) (bars represent standard deviation of the mean).*

solution of the inner film layer. Even if the dissolution mechanism is more severe when acting alone, the synergistic effect is thought to be dominated by mechanical removal enhanced by dissolution.

ACKNOWLEDGMENTS

Financial support for this work provided by the Australian Government in the form of an Australian Postgraduate Award Scholarship held by V. Ruzic is gratefully acknowledged.

REFERENCES

1. V. Ruzic, M. Veidt, S. Nešić, Corrosion 62, 5 (2006): p. 419.
2. V. Ruzic, M. Veidt, S. Nešić, Corrosion 62, 7 (2006): p. 598.
3. B. Chexal, J. Horowitz, B. Dooley, P. Millett, C. Wood, R. Jones, M. Bouchacourt, F. Remy, F. Nordmann, P. Saint Paul, W. Kastner, "Flow-Accelerated Corrosion in Power Plants," Joint Electric Power Research Institute, Inc., Electricite de France and Siemens AG Power Generation Report, TR-106611-R1, July, 1998.
4. F. Giralt, O. Trass, Can. J. Chem. Eng. 53, (1975): p. 505.
5. G. Schmitt, C. Bosch, U. Pankoke, W. Bruckoff, G. Siegmund, "Evaluation of Critical Flow Intensities for FILC in Sour Gas Production," CORROSION/98, paper no. 46 (Houston, TX: NACE International, 1998).
6. G. Schmitt, M. Mueller, "Critical Wall Shear Stress in CO_2 Corrosion of Carbon Steel," CORROSION/99, paper no. 44 (Houston, TX: NACE, 1999).
7. B.C. Syrett, Corrosion 32, 6 (1976): p. 242.
8. G. Schmitt, T. Gudde, E. Strobel-Effertz, "Fracture Mechanical Properties of CO_2 Corrosion Product Scales and Their Relation to Localized Corrosion," CORROSION/96, paper no. 9 (Houston, TX: NACE, 1996).
9. K.D. Efird, Corrosion 33, 1 (1977): p. 3.
10. D.C. Silverman, Corrosion 40, 5 (1984): p. 220.
11. F. Giralt, O. Trass, Can. J. Chem. Eng. 54, (1976): p. 148.
12. A. Dugstad, "The Importance of $FeCO_3$ Supersaturation on the CO_2 Corrosion of Carbon Steels," CORROSION/92, paper no. 14 (Houston, TX: NACE, 1992).
13. M.R. Crocker, P.G. Fairhurst, D.I. Wilson, "Model Experiments of Crystalline Scale Removal," The 1996 IChemE Research Event—2nd European Conf. for Young Researchers in Chemical Engineering, held April 2-3 (Leeds, U.K.: IChemE, 1996), p. 853.
14. C.J. Wilson, P.R. Lockyer, D.I. Wilson, "Modelling of Crystalline Scale Removal," Proc. Int. Conf. Mitigation of Heat Exchanger Fouling and Its Economic and Environmental Implications, ed. T.R. Bott, held July (Banff, AB, Canada: Begel House, Inc., 1999), p. 314.
15. S. Nešić, J. Postlethwaite, S. Olsen, Corrosion 52, 4 (1996): p. 285.
16. B. Vyas, "Erosion-Corrosion," in Treatise on Materials Science and Technology, vol. 16 (New York, NY: Academic Press Inc., 1979), p.357.
17. R.J.K. Wood, S.P. Hutton, Wear 140 (1990): p. 387.
18. S. Zhou, M.M. Stack, R.C. Newman, Corrosion 52, 12 (1996): p. 934.
19. F. Ferrer, H. Idrissi, H. Mazille, P. Fleischmann, P. Labeeuw, NDT&E Int. 33 (2000): p. 363.
20. D.D. He, X.X. Jiang, S.Z. Li, H.R. Guan, Corrosion 61, 1 (2005): p. 30.

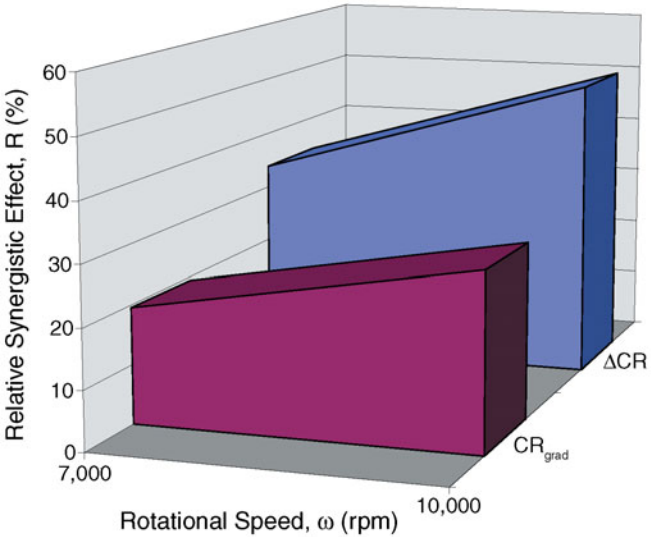

FIGURE 17. *Relative synergistic effect expressed via CR increments (ΔCR) and CR gradients (CR_{grad}).*